ACS APPLIED MATERIALS & INTERFACES

www.acsami.org

Research Article

Cupric Oxide Coating That Rapidly Reduces Infection by SARS-CoV-2 via Solids

Li-Meng Yan, Mohsen Hosseini, Alex W. H. Chin, Saeed Behzadinasab, Leo L. M. Poon,* and William A. Ducker*

ABSTRACT: The ongoing COVID-19 pandemic has created a need for coatings that reduce infection from SARS-CoV-2 via surfaces. Such a coating could be used on common touch surfaces (e.g., door handles and railings) to reduce both disease transmission and fear of touching objects. Herein, we describe the design, fabrication, and testing of a cupric oxide anti-SARS-CoV-2 coating. Rapid loss of infectivity is an important design criterion, so a porous hydrophilic coating was created to allow rapid infiltration of aqueous solutions into the coating where diffusion distances to the cupric oxide surface are short and the surface area is large. The coating was deposited onto glass from a dispersion of cuprous oxide in ethanol and then thermally treated at 700 °C for 2 h to produce a CuO coating that is ≈30 μm thick. The heat treatment oxidized the cuprous oxide to cupric oxide and sintered the particles into a robust film. The SARS-CoV-2 infectivity from the CuO film was reduced by 99.8% in 30 min and 99.9% in 1 h compared to that from glass. The coating remained hydrophilic for at least 5 months, and there was no significant change in the cross-hatch test of robustness after exposure to 70% ethanol or 3 wt % bleach.

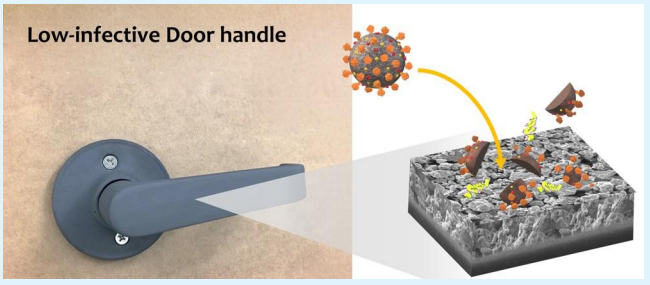

KEYWORDS: *SARS-CoV-2, coronavirus, coating, CuO, cupric oxide, viricidal, COVID-19*

1. INTRODUCTION

The coronavirus disease 2019 (COVID-19) was responsible for about 1,180,000 deaths[1] worldwide in the period of January−October 2020. With over 45 million cases, COVID-19 caused a dramatic change in human life and a dramatic downturn of the world economy in 2020. This disease is caused by a virus, SARS-CoV-2. The US Centers for Disease Control (CDC) has described the primary transmission mode to be via close contact or inhalation of respiratory droplets,[2] and research has suggested that airborne transmission is possible.[3] Infection from contaminated surfaces is known for other viruses[4] and occurs for SARS-CoV-2.[5] The CDC has recommended frequent disinfection of communal surfaces to reduce transmission.[2] Recent work has shown that SARS-CoV-2 remains viable on solids for extended periods; it is viable for up to 1 week on hard surfaces such as glass and stainless steel.[6,7] This has led to the widespread fear of touching communal objects that may have been touched by other individuals and widespread efforts to decontaminate surfaces during the COVID-19 pandemic.[8]

One way to reduce COVID-19 transmission via surfaces is to engineer coatings that inactivate SARS-CoV-2 and to use the coating on communal objects such as door handles, elevator buttons, and gas pumps. Possible applications extend to hospitals,[9] schools, public transportation, and so forth. The aim is for the coating to reduce the inactivation period from 1 week[6,7] to minutes or hours or whatever the expected interval is between users of the coated object. We have recently described a surface coating with cuprous oxide as the active ingredient that inactivates 99.9% of SARS-CoV-2 in 1 h.[10] The dramatic reduction in longevity of the virus from 1 week to 1 h on stainless steel or glass shows that coatings have the potential to effect disinfection between users of communal objects. Our efforts are now focused on identifying additional active materials and producing more rapid inactivation.

In this study, we have investigated a cupric oxide coating. Although cupric oxide (CuO) is not as common as cuprous oxide (Cu_2O) for antimicrobial use, previously reported antimicrobial[11−13] and antibacterial[14,15] properties suggest potential against SARS-CoV-2. A significant advantage of CuO is that the fully oxidized state enables sintering of particles into a porous coating with a very large surface area. The mechanism of antimicrobial and antibacterial properties of solid-state cupric oxide is not fully understood, but prior work suggests that it is unlikely that Cu^{2+} ion release controls the

Received: October 30, 2020
Accepted: January 4, 2021
Published: January 22, 2021

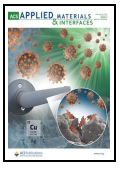

https://dx.doi.org/10.1021/acsami.0c19465
ACS Appl. Mater. Interfaces 2021, 13, 5919−5928

mechanism of damage to bacteria[16] due to the low solubility of CuO and the low amount of cupric ion release.[17] The high area of a sintered, porous film enables good contact between the virus and the CuO solid.

The practical use of CuO coating relies on its cytotoxicity properties. Semisch et al. investigated the cytotoxicity of CuO microparticles (<5 μm) against A549 and HeLa S3 cells after 24 h of incubation.[18] Their results did not show any sign of cytotoxic effect on either cells. Additionally, the median lethal dose (LD50) of cupric oxide is 2500 mg/kg (oral) and 2000 mg/kg (dermal) for rats, and no skin irritation or sensitization has been reported.[19]

In this work, we test the effect of a cupric oxide coating on suspensions of SARS-CoV-2 in aqueous droplets. We use viable SARS-CoV-2 and not a proxy virus, which means that experiments must be done under BSL-3 conditions that restrict the range of possible experiments. Use of active SARS-CoV-2 enables the demonstration of real applications to the ongoing COVID-19 pandemic. The infectivity was tested on Vero E6 cells, which are kidney cells from the African green monkey.

As described above, a key parameter is a short time period for inactivation in order to minimize the probability that deposited droplets can infect a future user of the contaminated object. The time taken includes the time for transport of the virus to the active ingredient in the film or for the active ingredient to diffuse to the virus. When the droplet lands on an impermeable solid, the diffusion length is initially approximately the size of the droplet. With time, the droplet evaporates, which lessens the required distance for transport and causes convection, which will also affect the transport.

To speed up the contact between the virus and the solid surface, we have designed a thin, porous, and hydrophilic CuO coating that draws aqueous droplets into its interior. Within the interior of the coating, the transport distances are much shorter (μm) than for a droplet sitting on the surface (mm). Drying times should also be shorter. Both these effects should speed the collision between the virus and the active surface. The interior space of the coating also has much greater contact area of the active ingredient than a planar surface. Our results show that the CuO coating reduced the infectivity by 99.8% in 30 min.

2. MATERIALS AND METHODS

2.1. Materials. Cuprous oxide microparticles HP III Type UltraFine-5 (95.6% Cu_2O, 3.2% CuO, and 0.1% Cu with trace amounts of lead, cadmium, and arsenic; mean particle size, 5.1 μm; and mode, 5.5 μm) were purchased from American Chemet Corporation. 100% ethanol (ACS grade), 70% ethanol (Reagent Grade), and glass slides (25 × 75 × 1 mm) were obtained from VWR. Stainless steel 302 shim, Precision Brand (unpolished ASTM A666; thickness, 0.3 mm) was purchased from Amazon website. The steel was cleaned with acetone and ethanol, and subsequently, washed with soap and water for 1 h. Concentrated bleach (7.5% sodium hypochlorite) was purchased from Kroger Supermarket and water was from a Milli-Q Reference water purification system.

2.2. Fabrication of CuO Coatings. CuO thin coatings were prepared by thermal oxidation of Cu_2O, followed by sintering. A 10% Cu_2O in ethanol suspension was sonicated for 6 min to yield a uniform dispersion. Glass slides were cut into 12 × 12 mm pieces, rinsed with 100% ethanol, and then 0.1 mL of Cu_2O suspension was applied on the surface. At this point, samples were left to dry at room temperature for approximately 20 min and then heat-treated in a furnace at 120 °C for 10 min, 350 °C for 10 additional minutes, and 700 °C and for 2 h to oxidize and undergo early-stage sintering to create necks between the particles. The furnace thermostat was returned to room temperature and the coated samples were cooled slowly overnight. Thick CuO coatings were prepared with the same procedure, but 0.2 mL of 16% Cu_2O in ethanol suspension was deposited on 15 × 15 mm glass initially. The conversion from cuprous to cupric oxide was obvious from the change in color of the coating from red-brown to graphite-colored. The railings and handles shown in the Supporting Information were sintered at 400 °C because we found that this was sufficient to form a robust coating.

2.3. Characterization of Coatings. *2.3.1. XRD, XPS, and SEM.* The X-ray diffraction (XRD) patterns obtained from a Bruker D8 ADVANCE diffractometer (monochromatic Cu Kα X-rays, wavelength = 1.5418 Å) were used to identify the structure of the oxidation product. X-ray photoelectron spectroscopy (XPS; PHI VersaProbe III with a monochromatic Al Kα source of 1486.6 eV) and electron-dispersive X-ray spectroscopy (EDX; Bruker Quantax) were used to study the chemical composition of the surface of the coating. Scanning electron microscopy (SEM; FEI Quanta 600FE-ESEM) was utilized to examine the coating morphology and coating thickness.

2.3.2. Contact Angle Measurements. The coating was designed to be hydrophilic to enhance the contact area between the droplet and the surface of CuO. The contact angle of 5 μL of water was measured using a First Ten Angstroms FTA125. The FTA instrument was also used to generate the images of imbibition.

2.3.3. ASTM D3359 Adhesion Test. The adhesion performance of CuO coatings on substrates was assessed according to Section 13 of ASTM D3359 standard code[20] using a cross-hatch grid. An 11 × 11 grid of cuts spaced 1 mm apart was made on samples. The surface was cleaned with an ultra-soft brush and then a piece of tape was applied on the grid and rubbed with a rubber eraser to ensure uniform contact. After 90 s of application, the tape was removed swiftly, while it was bent by about 180°. Subsequently, the area was inspected using an illuminated magnifier and rated on a scale of 0B to 5B, with 5B assigned for perfect adhesion, to evaluate the adhesion performance according to the standard ASTM D3359 classification of adhesion chart.

2.3.4. Disinfection/Adhesion Test. A variant of ASTM D3359 method B was used to evaluate the robustness of CuO coating when disinfected. After inscribing the cross-cut pattern, the coating was soaked in 70% ethanol or 3% bleach for 20 min and then dried before applying the tape.

2.3.5. Drying Time. The test solid was placed on a weighing balance with 0.1 mg resolution (A&D Company). A 5 μL drop was placed on the solid at 22 °C and 35% relative humidity (RH), and the mass was measured at 1 min intervals until the mass dropped below the resolution of the balance. The results are average of three tests for saliva; each of the three tests used saliva from a different individual.

2.4. SARS-COV-2 Inactivation Test. Vero E6 cells were used to prepare virus stock and to test the viability of the virus by microscopic observation of the cytopathic effect caused by the virus. The cells were cultured at 37 °C and 5% CO_2 in 2% fetal bovine serum and 1% v/v penicillin−streptomycin in Dulbecco's modified Eagle's medium. The Hong Kong index SARS-COV-2 virus was used in the tests and 0.5% (w/v) bovine serum albumin and 0.1% (w/v) glucose in Earle's balanced salt solution with a pH of 7.4 was used as a viral transport medium.

Inactivation of the virus by the CuO coating was examined as follows. The CuO or control coating was initially disinfected with 70% ethanol in water, followed by drying in an air atmosphere at 37 °C overnight. A 5 μL droplet containing 6.2 × 10^7 (7.8 log unit) $TCID_{50}$/mL of the virus was spotted on the test solid at 22−23 °C and 60−70% humidity, and after a predefined time, the coating was immersed in 300 μL of viral transport medium to elute the virus. The active virus within the eluted droplet was assessed using a 50% tissue culture infective dose ($TCID_{50}$) assay[21,22] using Vero E6 cells. The $TCID_{50}$ assay consists of making a series of 3.16× (i.e., half-log) dilutions of the eluted virus. Cells on 96-well plates were exposed to one of the dilutions, with quadruplicate[23] of each dilution. The cells were then incubated at 37 °C and 5% CO_2. After 5 days, the cells were assessed for any cytopathic effect. The dilution at which 50% (2 of 4) of Vero E6 cell cultures showed a cytopathic sign is called

https://dx.doi.org/10.1021/acsami.0c19465
ACS Appl. Mater. Interfaces 2021, 13, 5919−5928

$TCID_{50}$/mL. Three independent samples (i.e., a new solid sample and a new inoculation of virus) were tested for each time point, and the virus inactivation at each time point was calculated based on the reduction of log($TCID_{50}$/mL) as follows

$$\text{log reduction} = \text{mean}\left(\log_{10}\frac{\text{control titer}}{\text{sample titer}}\right) \quad (1)$$

units

units

primary elements, with the elemental composition of the surface being 47.5% O, 40% Cu, 9.2% C, 1.7% Cl, and 1.6% Na. Carbon is a common contaminant identified in XPS spectra. The oxidation state of Cu was identified from the Cu $2p_{3/2}$ spectrum (Figure 2B), which contained a broad peak at 932−934 eV and a characteristic satellite feature of CuO at 940−945 eV.

The peak at 932−934 eV was deconvoluted into two peaks at 932.6 and 933.8 eV (E_b). The peak at 933.8 eV was assigned

https://dx.doi.org/10.1021/acsami.0c19465
ACS Appl. Mater. Interfaces 2021, 13, 5919−5928

dilution for CuO sample
dilution for uncoated sample

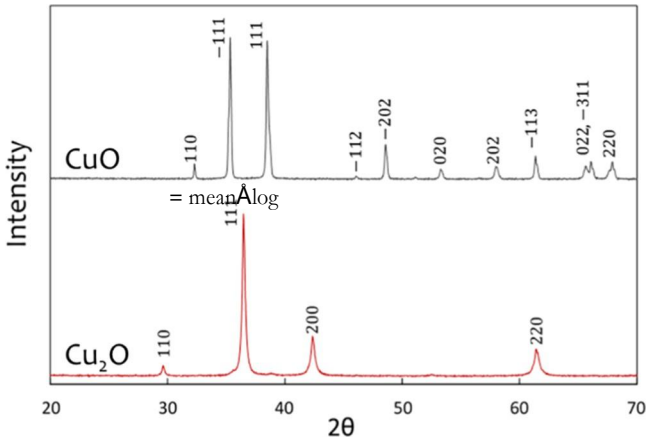

= mean log

to CuO and the peak at 932.6 eV could be from either Cu

https://dx.doi.org/10.1021/acsami.0c19465
ACS Appl. Mater. Interfaces 2021, 13, 5919−5928

$$\% \text{ reduction} = (1 - 10^{-\log \text{ reduction}}) \times 100 \quad (2)$$

https://dx.doi.org/10.1021/acsami.0c19465
ACS Appl. Mater. Interfaces 2021, 13, 5919−5928

modified Auger parameter[28] of 1851.7 eV (E_b + E_k) was in

https://dx.doi.org/10.1021/acsami.0c19465
ACS Appl. Mater. Interfaces 2021, 13, 5919−5928

2D) was used to distinguish between these two possibilities. The single peak with a kinetic energy of 917.9 eV (E_k) gave a

excellent agreement with the known value of CuO (1851.7

https://dx.doi.org/10.1021/acsami.0c19465
ACS Appl. Mater. Interfaces 2021, 13, 5919−5928

https://dx.doi.org/10.1021/acsami.0c19465
ACS Appl. Mater. Interfaces 2021, 13, 5919−5928

https://dx.doi.org/10.1021/acsami.0c19465
ACS Appl. Mater. Interfaces 2021, 13, 5919−5928

https://dx.doi.org/10.1021/acsami.0c19465
ACS Appl. Mater. Interfaces 2021, 13, 5919−5928

https://dx.doi.org/10.1021/acsami.0c19465
ACS Appl. Mater. Interfaces 2021, 13, 5919−5928

https://dx.doi.org/10.1021/acsami.0c19465
ACS Appl. Mater. Interfaces 2021, 13, 5919−5928

https://dx.doi.org/10.1021/acsami.0c19465
ACS Appl. Mater. Interfaces 2021, 13, 5919−5928

https://dx.doi.org/10.1021/acsami.0c19465
ACS Appl. Mater. Interfaces 2021, 13, 5919−5928

https://dx.doi.org/10.1021/acsami.0c19465
ACS Appl. Mater. Interfaces 2021, 13, 5919−5928

https://dx.doi.org/10.1021/acsami.0c19465
ACS Appl. Mater. Interfaces 2021, 13, 5919−5928

https://dx.doi.org/10.1021/acsami.0c19465
ACS Appl. Mater. Interfaces 2021, 13, 5919−5928

https://dx.doi.org/10.1021/acsami.0c19465
ACS Appl. Mater. Interfaces 2021, 13, 5919−5928

https://dx.doi.org/10.1021/acsami.0c19465
ACS Appl. Mater. Interfaces 2021, 13, 5919−5928

https://dx.doi.org/10.1021/acsami.0c19465
ACS Appl. Mater. Interfaces 2021, 13, 5919−5928

https://dx.doi.org/10.1021/acsami.0c19465
ACS Appl. Mater. Interfaces 2021, 13, 5919−5928

https://dx.doi.org/10.1021/acsami.0c19465
ACS Appl. Mater. Interfaces 2021, 13, 5919−5928

https://dx.doi.org/10.1021/acsami.0c19465
ACS Appl. Mater. Interfaces 2021, 13, 5919−5928

https://dx.doi.org/10.1021/acsami.0c19465
ACS Appl. Mater. Interfaces 2021, 13, 5919−5928

https://dx.doi.org/10.1021/acsami.0c19465
ACS Appl. Mater. Interfaces 2021, 13, 5919−5928

https://dx.doi.org/10.1021/acsami.0c19465
ACS Appl. Mater. Interfaces 2021, 13, 5919−5928

https://dx.doi.org/10.1021/acsami.0c19465
ACS Appl. Mater. Interfaces 2021, 13, 5919−5928

https://dx.doi.org/10.1021/acsami.0c19465
ACS Appl. Mater. Interfaces 2021, 13, 5919−5928

https://dx.doi.org/10.1021/acsami.0c19465
ACS Appl. Mater. Interfaces 2021, 13, 5919−5928

https://dx.doi.org/10.1021/acsami.0c19465
ACS Appl. Mater. Interfaces 2021, 13, 5919−5928

https://dx.doi.org/10.1021/acsami.0c19465
ACS Appl. Mater. Interfaces 2021, 13, 5919−5928

https://dx.doi.org/10.1021/acsami.0c19465
ACS Appl. Mater. Interfaces 2021, 13, 5919−5928

https://dx.doi.org/10.1021/acsami.0c19465
ACS Appl. Mater. Interfaces 2021, 13, 5919−5928

https://dx.doi.org/10.1021/acsami.0c19465
ACS Appl. Mater. Interfaces 2021, 13, 5919−5928

https://dx.doi.org/10.1021/acsami.0c19465
ACS Appl. Mater. Interfaces 2021, 13, 5919−5928

https://dx.doi.org/10.1021/acsami.0c19465
ACS Appl. Mater. Interfaces 2021, 13, 5919−5928

https://dx.doi.org/10.1021/acsami.0c19465
ACS Appl. Mater. Interfaces 2021, 13, 5919−5928

https://dx.doi.org/10.1021/acsami.0c19465
ACS Appl. Mater. Interfaces 2021, 13, 5919−5928

https://dx.doi.org/10.1021/acsami.0c19465
ACS Appl. Mater. Interfaces 2021, 13, 5919−5928

https://dx.doi.org/10.1021/acsami.0c19465
ACS Appl. Mater. Interfaces 2021, 13, 5919−5928

https://dx.doi.org/10.1021/acsami.0c19465
ACS Appl. Mater. Interfaces 2021, 13, 5919−5928

https://dx.doi.org/10.1021/acsami.0c19465
ACS Appl. Mater. Interfaces 2021, 13, 5919−5928

https://dx.doi.org/10.1021/acsami.0c19465
ACS Appl. Mater. Interfaces 2021, 13, 5919−5928

https://dx.doi.org/10.1021/acsami.0c19465
ACS Appl. Mater. Interfaces 2021, 13, 5919−5928

https://dx.doi.org/10.1021/acsami.0c19465
ACS Appl. Mater. Interfaces 2021, 13, 5919−5928

https://dx.doi.org/10.1021/acsami.0c19465
ACS Appl. Mater. Interfaces 2021, 13, 5919−5928

https://dx.doi.org/10.1021/acsami.0c19465
ACS Appl. Mater. Interfaces 2021, 13, 5919−5928

https://dx.doi.org/10.1021/acsami.0c19465
ACS Appl. Mater. Interfaces 2021, 13, 5919−5928

https://dx.doi.org/10.1021/acsami.0c19465
ACS Appl. Mater. Interfaces 2021, 13, 5919−5928

https://dx.doi.org/10.1021/acsami.0c19465
ACS Appl. Mater. Interfaces 2021, 13, 5919−5928

https://dx.doi.org/10.1021/acsami.0c19465
ACS Appl. Mater. Interfaces 2021, 13, 5919−5928

https://dx.doi.org/10.1021/acsami.0c19465
ACS Appl. Mater. Interfaces 2021, 13, 5919−5928

https://dx.doi.org/10.1021/acsami.0c19465
ACS Appl. Mater. Interfaces 2021, 13, 5919−5928

https://dx.doi.org/10.1021/acsami.0c19465
ACS Appl. Mater. Interfaces 2021, 13, 5919−5928

https://dx.doi.org/10.1021/acsami.0c19465
ACS Appl. Mater. Interfaces 2021, 13, 5919−5928

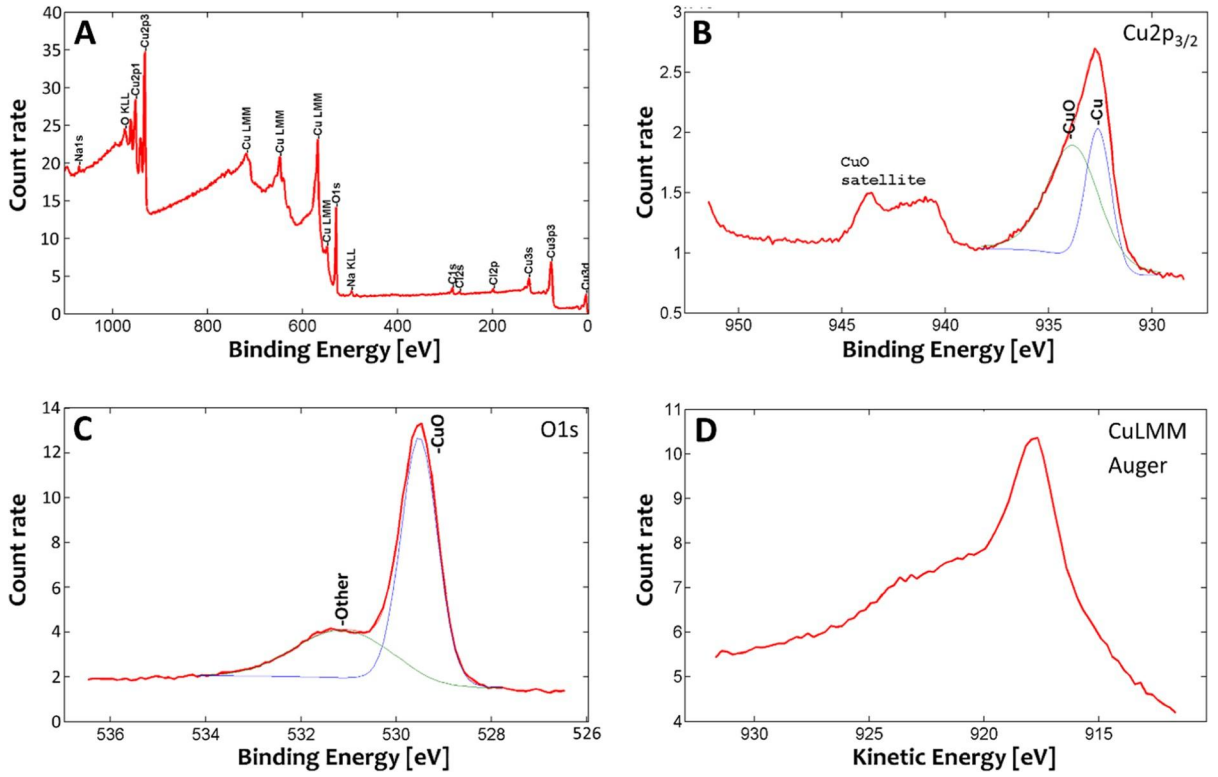

Figure 2. XPS results of the fabricated CuO coating. (A) Survey spectrum showing the preponderance of copper and oxygen on the surface. (B) Cu $2P_{3/2}$ spectrum. The deconvoluted peaks are shown for both Cu (blue) and CuO (green), as labeled. (C) Oxygen spectrum. The deconvoluted peaks are shown for both CuO (blue) and other oxygen species (green) as labeled. (D) CuLMM Auger kinetic energy. The vertical axis is the electron count rate in units of 10000 counts per second.

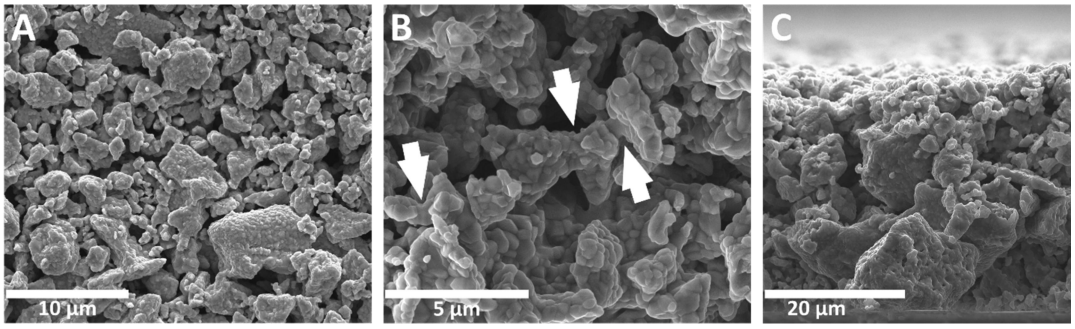

Figure 3. SEM images of cupric oxide films. (A) Plane view of the coating showing the porosity. (B) Higher magnification showing the necks (indicated by arrows) produced by early-stage sintering of particles. (C) Cross-sectional view of the coating.

detection limit, which was <99% reduction compared to the 0 h time point.[7] After only 30 min, there was already a large viable virus reduction on the CuO coating compared to that on the uncoated glass: on average, 99.8%. The 95% CI for the reduction at 30 min shows that more than 93.1% of the virus was inactivated (one tailed and heteroscedastic, calculated using R software).

When the virus was deposited onto a porous surface, the ability to infect cells can be affected in two ways: (a) from inactivation using an active material and (b) from the virus becoming trapped or adsorbed onto an area of high porosity and not recovered by the subsequent elution. We investigated the effect of the porous area by making a thicker CuO coating using the same method but with 2.2× mass of particles per unit area compared to the previous samples such that the entire droplet was, within seconds, imbibed into the film. On this thicker film (Figure 4B), a dramatic decrease in the ability of the virus to infect Vero E6 cells was found. Immediately (≈1 min) after deposition of the droplet, the reduction was 99.6% (95% CI, >94.2%) compared to that on glass, and after 30 min, the virus was below the detection limit. Clearly, this thick porous coating is a very effective way of reducing the ability of a solid to infect cells. All other tests in this paper are for the original (thinner) coating.

The results demonstrate very rapid reduction of infection by SARS-CoV from a coating that can be used on objects such as metal door handles that can be heat-treated. In practice, we found that sintering on such objects could be achieved at 400 °C, and examples are shown in Figure S3, Supporting Information. Later, we also show that the coating is very robust, as expected for a sintered coating of mineral particles.

3.3. Material Leaching from the Coating Does Not Inactivate SARS-CoV-2. The study of the mechanism of inactivating SARS-CoV-2 by cupric oxide is beneficial for the

https://dx.doi.org/10.1021/acsami.0c19465
ACS Appl. Mater. Interfaces 2021, 13, 5919−5928

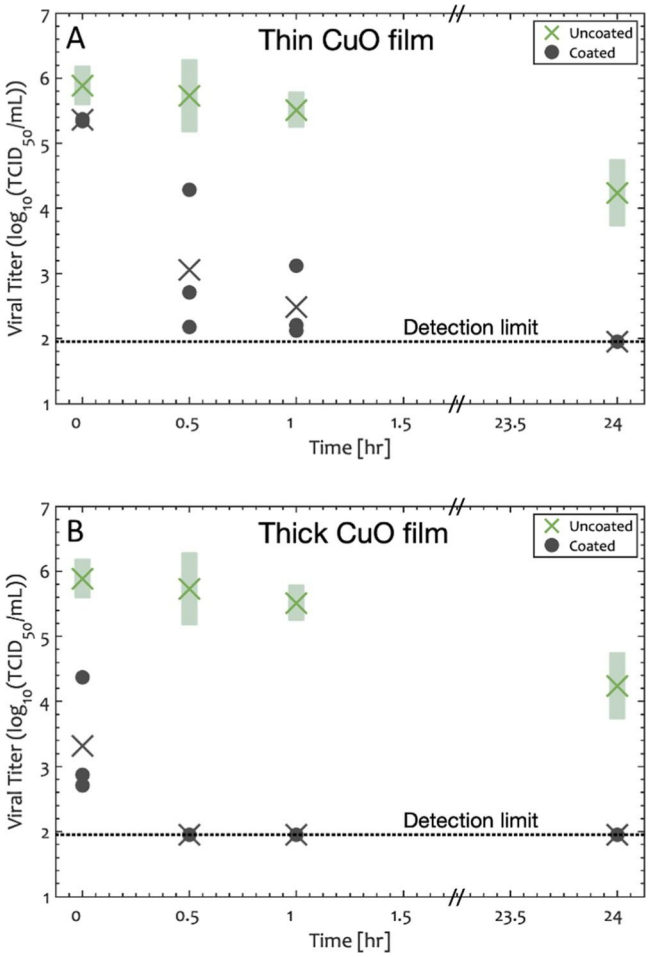

Figure 4. (A) Viable virus titer on thin CuO coating and comparison with plain glass at different time periods. × represents the average of the log of the viral titer at each time, black circles represent individual data points measured on CuO, and the dashed line shows the detection limit of 90 $TCID_{50}$/mL. There are many data points for glass, including some reproduced from ref 10, so the glass data are shown by a shaded green rectangle representing the 95% CI. The inactivation of SARS-CoV-2 is much faster on the CuO films than on plain glass: 99.8% greater at 30 min ($p = 2.5 \times 10^{-2}$ compared to that on glass at the same time) and 99.9% greater in 1 h ($p = 4.4 \times 10^{-3}$) for the thin CuO film. (B) Data for the thick film are superior to those for the thin film: 99.7% reduction compared to that on glass within 1 min ($p = 0.0189$), 99.9% reduction at 30 min ($p = 2.3 \times 10^{-4}$) and 99.9% reduction in 1 h ($p = 6.4 \times 10^{-12}$).

design of future antiviral coatings and surfaces. A number of reviews have summarized how copper may attack pathogens, and the mechanisms include the release of cupric ions,[36−38] production of reactive oxygen species (ROS),[38−40] surface catalysis, or contact killing with the solid.[36−39,41] Herein, we describe a test to evaluate the antiviral property of species that are leached from our coating or created by our coating. The hypothesis was that the virus was inactivated by species that are dissolved or suspended in the liquid after contact with the solid, and it was tested by exposing the virus to the leachate from the film, without exposing the virus to the coating itself. The CuO coating was initially soaked in 300 μL of viral culture medium (without any virus) for 24 h at room temperature. Next, 135 μL of the medium was mixed with 15 μL of the virus and the mixture was incubated at room temp for 1 h (the time period required for more than 99.9% inactivation by the film) or 24 h (an exaggerated time scale to allow for more subtle effects) before assessing the viability of SARS-CoV-2 to infect Vero E6 cells via the standard $TCID_{50}$ measurement. Note that the virus was never in contact with the coating. This protocol was similar to that reported by Sunada et al.[39]

The results shown in Figure 5 demonstrate that the infectivity of the virus was about the same when it was

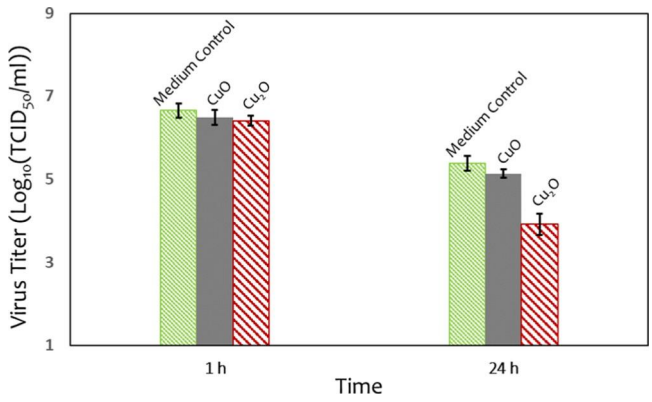

Figure 5. Effect of equilibration with leachate from coating for 1 or 24 h on the viability of SARS-CoV-2. Three different liquids are compared: the medium (negative control), leachate from the CuO coating, and leachate from Cu_2O coating (positive control). The virus was never in contact with the solid. Leachate from CuO did not significantly inactivate the virus, even over 24 h of exposure.

exposed to the CuO leachate or culture medium ($p = 0.73$, ANOVA with two factors time and solid). In contrast, when Cu_2O coating was tested instead of a CuO coating, the $TCID_{50}$/mL was reduced by over 10×, indicating that our experiment had the capability to resolve a reduction (positive control, $p = 0.01$). The hypothesis that dissolved material was the cause of inactivation was rejected, and we conclude that the contact between SARS-CoV-2 and CuO is necessary to inhibit infection. Our findings are consistent with the previously reported results for the antibacterial properties of CuO.[16,17] The reduction in infectivity of CuO coating is similar to that of Cu_2O, even though CuO acts without the assistance of inactivation via a leachate.

Contact inactivation of SARS-CoV-2 by CuO may be aided by an attractive charge−charge interaction. The culture medium has an ionic strength of about 0.15, which corresponds to a Debye-length of about 0.8 nm, which is still sufficiently long for electrostatic interactions to occur in a short range. The spike proteins which protrude furthest from the envelope have 10 cationic amino acids, 7 anionic amino acids, and 1 histidine,[42] giving a net charge of about positive 3.5 at pH 7.4. The envelope (*E*) protein also has a net positive charge.[43] Cupric oxide has a negative zeta potential (−17 mV) in the culture medium.[44] SARS-CoV-2 should therefore be attracted to cupric oxide via an electrostatic interaction. It is also possible that this charge−charge interaction may be part of the mechanism of inactivation.

3.4. Film is Robust and the Wetting Properties Do Not Age. *3.4.1. Contact Angle Measurements.* The CuO coating has been designed and engineered to be hydrophilic to rapidly draw in the infected droplet and inactivate the virus. We have recently reported a cuprous oxide-based anti-SARS-COV-2 coating that loses its hydrophilicity over time because of the presence of polyurethane.[10] We would expect the

https://dx.doi.org/10.1021/acsami.0c19465
ACS Appl. Mater. Interfaces 2021, 13, 5919−5928

cuprous oxide coating to have improved performance if it were to remain hydrophilic and therefore allow imbibition into the coating. Here, we designed a coating without polyurethane so that it would not age or have polyurethane covering on part of the active surface. Figure S4, Supporting Information, illustrates that the hydrophilic nature of the coating was maintained over a 5 month period. A water droplet rapidly wets and imbibes at any time during the 5 month test period, and the advancing, sessile, and receding contact angles were <10°.

3.4.2. ASTM D3359 Adhesion Tests. We foresee possible applications where the CuO coating could be used on store door handles, public transportation railings, and perhaps railings in medical environments that are sometimes made of steel (see Figure S3, Supporting Information). Because such hand holds are commonly disinfected during the pandemic, we tested whether the coating retained its physical integrity after exposure to common disinfectants using the ASTM D3359 method B where the adhesion was assessed in combination with disinfection by either 70% ethanol or 3% bleach in water. Approximately, 1 in. square pieces of stainless steel 302 were cross-hatched according to ASTM D3359-B, then exposed to the disinfectant, and then the adhesion was tested. The test was conducted on three independent samples for each disinfection condition. Figure S5, Supporting Information, shows images of an inscribed grid before and after applying the tape. The cross-hatching creates initiation sites for coating failure but damage to these sites was very low: the average percentage of affected cells was 0.67% (no disinfection), 1.3% (3% bleach), and 0.5% (70% ethanol). The coating was rated 4B according to the standard ASTM D3350 classification of adhesion.[20]

4. DISCUSSION

4.1. Factors Affecting the Inactivation Time. In principle, the time to inactivate the virus depends on two rates: the rate of transport to the active surface and the rate inactivation by the active ingredient. If transport is the rate- limiting step, then there is little point in accelerating the inactivation on contact. In general, the transport time is complex to calculate for a drying droplet on a surface. First, the transport depends on the mechanism. If the virus is inactivated by contact with a fixed solid, transport of the virus is the relevant quantity, whereas if inactivation is caused by dissolved ions, then the transport of the dissolved ions should be considered, as well as the time taken for dissolution to occur. When considering transport, we assume that the diffusion coefficient is given by the Stokes−Einstein equation

$$D = \frac{kT}{6\pi\eta r} \quad (3)$$

where k is the Boltzmann constant, T is the temperature, η is the viscosity, and r is the radius. The diffusion constant is inversely proportional to the radius of species being transported. Therefore, the diffusion of virus will be much slower than that of ions because the virus has a much greater radius (~50 nm, including spike proteins[45,46]) than that of metal ions (~0.5 nm), and transport is more limiting for contact inactivation than for ion dissolution. As our data are consistent with the mechanism of contact inactivation, we will focus on the effect of drying on the transport of the virus to the solid.

The diffusion distance in a droplet depends on the droplet size and contact angle of the droplet on the solid (Figure 6). A

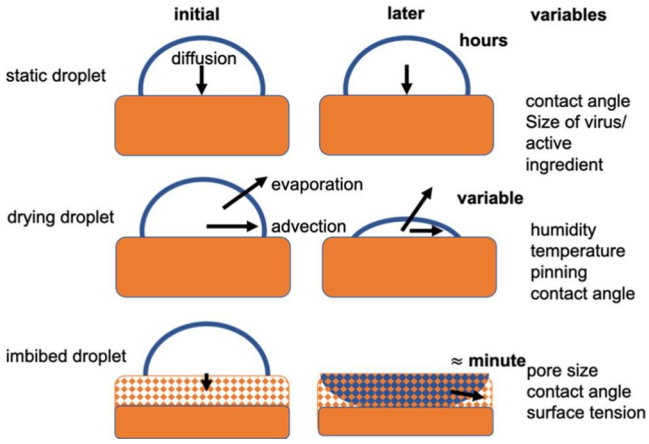

Figure 6. Schematic of various modes of enabling contact between the virus and the active surface. A drying droplet is superior to a static droplet because of advection and a smaller volume. Imbibition quickly brings the viral suspension into close contact with the active material and therefore reduces transport times. The imbibed droplet also dries more quickly as shown in Figure 8.

large range of sizes is reported for respiratory droplets in air: <1 to 100 μm, for talking and coughing,[47−51] and much larger for sneezing, 300−900 μm,[52] or even mm in size,[53] which means that if spherical, the typical dimension is about 1 mm. The smaller droplets are more likely to evaporate quickly before settling, so the larger droplets which are deposited (>10 μm) are most important here. Therefore, our 5 μL ($r \approx 1$ mm) test droplets are at the larger but still relevant end of the spectrum. The initial contact angle on an impermeable surface also has an effect: the lower the angle, the smaller the average diffusion distance. Using a typical diffusion distance of 0.5 mm, the viscosity of saliva ≈ 0.07 N s m^{-2},[54,55] and approximating to planar diffusion from the center of the droplet, the diffusion time will be on the order of many hours. For a non-evaporating sessile droplet on an impermeable solid, we cannot rely on diffusion alone to carry the virus to the surface of a film between two subsequent users of a communal object such as a door handle.

Drying of the droplet will clearly be a major factor in bringing the virus into contact with the solid. Deposition of particles onto impermeable solids from an evaporating droplet has been studied extensively, especially the phenomenon known as the "coffee ring effect".[56−58] The deposition depends on the presence of surface active agents and other species in the droplet.[59] For respiratory droplets, there will be biological polymers, salts, and other ingredients. In brief, evaporation of the liquid not only leads to a diminishing droplet volume but also sets up flows within the droplet, which together with surface tension gradients affect the deposition. The diminishing size of the droplet and convection will speed up the transport to the surface. In the final stages of drying, the concentration of any leachate may climb dramatically, if dissolution is out of equilibrium. The overall drying will depend strongly on the temperature and the humidity.

By creating a porous hydrophilic film that imbibes the droplet, as we have done here, the situation is changed considerably (Figure 6). The most important point is that, instead of diffusion over the millimeter scale of the droplet,

https://dx.doi.org/10.1021/acsami.0c19465
ACS Appl. Mater. Interfaces 2021, 13, 5919−5928

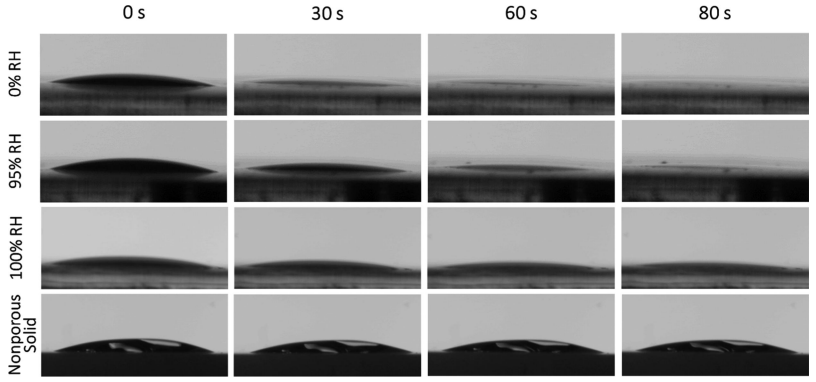

Figure 7. Imbibition of a 5 μL water droplet by porous CuO coatings as a function of time and RH. Even at 95% humidity, a 5 μL droplet is imbibed within about 80 s. Imbibition at 0% humidity (complete at about ~60 s), at 100% humidity (no imbibition at 80 s) and for a non-porous solid (no imbibition) shown for comparison.

once imbibition occurs, diffusion of the virus only needs to occur over the designed size of the pore, which here is on the order of micrometers. This 1000-fold reduction in scale should make diffusion tenable for driving the contact of the virus with the active surface. In addition, imbibing into a porous film reduces the vicissitudes of the local temperature and humidity that are critical if drying is used to draw the virus into contact with an active impermeable solid. Clearly, for hot, low humidity conditions, droplets will dry very quickly and draw the virus into contact with the solid, but at high humidity drying will be slow.

Imbibition into our coating would not be as effective if the pore space were already filled with water that condenses from the air. The Kelvin equation suggests that capillary condensation will only occur for large pores (≈μm) as the humidity approaches 100%. The calculation would require detailed knowledge of the pore geometry, which in this case is inhomogeneous; here, we simply measured the imbibition of water into our CuO coating as a function of humidity. Our results show that, in the range of 0−95% humidity, a 5 μL droplet is imbibed into the film within 80 s (see Figure 7), which is a suitable transport time for viral inactivation and suggests that the coating will be deployable over most of the normal range of humidity conditions. In fact, imbibition is not much slower at 95% humidity than at 0% humidity.

Although very small pores are advantageous for creating small diffusion distances, the viscous drag is important for imbibing the liquid into the solid. This should be considered for respiratory droplets. The Washburn equation approximates the distance travelled, L, into a pore of the coating for a given time

$$L = \sqrt{\frac{\gamma r_p \cos\theta}{2\eta} \cdot t} \tag{4}$$

where γ is the solid−liquid interfacial tension, r_p is the radius of the pore, θ is the contact angle, and t is the time. More sophisticated treatments that include the tortuosity of the film[60−63] are described in the Supporting Information; the trends are similar, but the calculated imbibition is generally slower.

Our results showed that imbibition of 5 μL water into our coating was complete within about 80 s, which is a suitable time for inactivation of SARS-CoV-2. The r_p/η scaling of L in eq 4 suggests that imbibition of more viscous liquids, such as saliva (≈0.07 N s m^{-2}[54,55] = 70 × water viscosity) that contains SARS-CoV-2, may require larger pore sizes to achieve similar imbibition times.

4.2. Additional Effects of Porous Film. A porous film provides a much greater surface area than that of a smooth film. Whether the mechanism is contact inactivation or dissolution, the greater surface area is beneficial for inactivation via one of these surface processes. In addition, the porous surface provides an opportunity for faster drying of a droplet.[64,65] Faster drying reduces the time taken to pull the suspended virus into proximity with the active surface. In Figure 8 we compare the drying time on the porous CuO coating with that on the uncoated (no-porous) solid for both water and droplets of human saliva. For both saliva and water, the drying rate was about 3 times as fast on the CuO film. On the CuO film, the droplet is effectively dry after about 6 min. Drying aids the process of pulling the virus into contact with the solid, and drying readies the surface for subsequent respiratory droplets. Improved drying time is therefore a

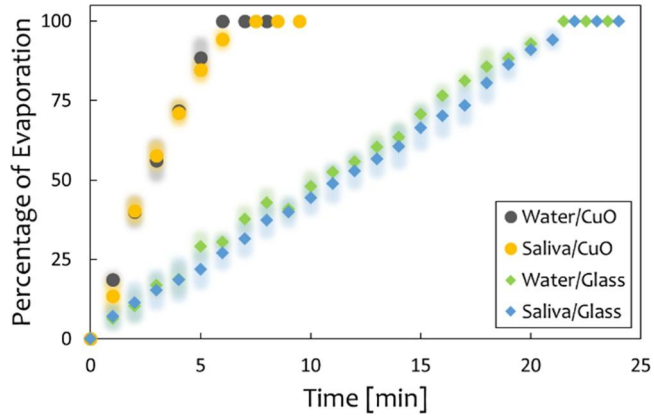

Figure 8. Drying of a 5 μL droplet on CuO porous coating on glass compared to the drying time on non-porous glass at 22 °C and 35% RH. Symbols indicate average values, and the shaded regions depict the standard deviation at each time point for three replicates. The average drying rates are 16.9 ± 0.2 percent/min for water/CuO, 13.7 ± 0.7 for saliva/CuO, 4.6 ± 0.1 for water/glass, and 4.34 ± 0.08 for saliva/glass. The drying rate of a droplet on the porous CuO film is thus about 3 times faster for both pure water (Student's t-test, one tail unpaired $p = 1.3 \times 10^{-4}$) and for saliva (Student's t-test, one tail unpaired $p = 1.1 \times 10^{-3}$).

https://dx.doi.org/10.1021/acsami.0c19465
ACS Appl. Mater. Interfaces 2021, 13, 5919−5928

significant advantage of a porous film for reducing transmission to subsequent users of communal objects.

An additional advantage of a porous film is that the active surface within the pore structure is provided with a degree of protection from abrasions and other insults that occur to the surface layers during normal usage. For comparison, molecular layers on an impermeable surface coating may be subject to rapid wear with associated loss of effectiveness.

4.3. Practical Applications of Sintered CuO Coating.

The coating, as prepared by sintering, requires the underlying material to withstand a temperature of 400 °C, which places some limits on its application. We found that commercial steel door handles and railing could be coated at this temperature (Figure S3) as well as on glass and silicon. We made the coating from Cu_2O, which in 2020 cost about $16/kilogram, or about 1/50th of the cost of silver, which is a common antimicrobial ingredient.

5. CONCLUSIONS

We have fabricated a CuO coating that reduces infection from SARS-CoV-2 suspended in 5 μL droplets that are deposited on the coating. The infectivity from SARS-CoV-2 in the CuO film is reduced by, on average, 99.9% in 60 min and the 95% CI is >99.26% decrease in infectivity compared to that on glass. The reduction is even greater for a thicker film that immediately imbibes the entire droplet. The coating was fabricated from a dispersion of Cu_2O that was heat-treated in air at 700 °C to produce CuO and to create a robust coating with contacts between the particles formed by early-stage sintering. Leachate from the coating did not reduce the infectivity of SARS-CoV-2, consistent with a mechanism of viral inactivation by contact with the solid. The measured reduction in infectivity is swift for a non-soluble material. The coating is hydrophilic and porous and achieves rapid imbibition and rapid drying of small droplets. It remains hydrophilic for at least 5 months and is resistant to debonding from steel, as demonstrated by a cross-hatch test. The addition of a porous coating increased the drying rate by a factor of 3, a drying enhancement that may find other applications.

ASSOCIATED CONTENT

Supporting Information

The Supporting Information is available free of charge at https://pubs.acs.org/doi/10.1021/acsami.0c19465.

Surface elemental analysis of coating by EDS; TCID50/mL assay results of Figure 4 and results for glass; image of the coating before oxidation and after oxidation at 700 °C for 2 h; a comparison of particle structure of cuprous oxide particles (not heat-treated and bound by polyurethane) and cupric oxide (heat-treated); a steel hand rail and door handles with a porous anti-SARS-CoV-2 coating of cupric oxide (graphite colored) and without the coating (steel colored); contact angle of the cupric oxide film in the course of time; photographs of cross-hatch test results for CuO films; and calculations of imbibition of a droplet into a tortuous porous medium (PDF)

AUTHOR INFORMATION

Corresponding Authors

Leo L. M. Poon − *School of Public Health, LKS Faculty of Medicine and HKU-Pasteur Research Pole, LKS Faculty of Medicine, The University of Hong Kong, Hong Kong, China*; Email: llmpoon@hku.hk

William A. Ducker − *Dept. of Chemical Engineering and Center for Soft Matter and Biological Physics, Virginia Tech, Blacksburg, Virginia 24061, United States*; orcid.org/0000-0002-8207-768X; Email: wducker@vt.edu

Authors

Mohsen Hosseini − *Dept. of Chemical Engineering and Center for Soft Matter and Biological Physics, Virginia Tech, Blacksburg, Virginia 24061, United States*

Alex W. H. Chin − *School of Public Health, LKS Faculty of Medicine, The University of Hong Kong, Hong Kong, China*; orcid.org/0000-0002-6556-9092

Saeed Behzadinasab − *Dept. of Chemical Engineering and Center for Soft Matter and Biological Physics, Virginia Tech, Blacksburg, Virginia 24061, United States*

Complete contact information is available at: https://pubs.acs.org/10.1021/acsami.0c19465

Notes

The authors declare no competing financial interest.

ACKNOWLEDGMENTS

The authors thank Stephen McCartney for capturing the SEM images and acknowledge the use of Electron Microscopy facilities within the Nanoscale Characterization and Fabrication Laboratory at Virginia Polytechnic Institute and State University. The authors also thank Xu Feng for capturing the XPS spectra and acknowledge the use of Surface Analysis Laboratory in the Department of Chemistry at Virginia Tech, which was supported by the National Science Foundation under grant no. CHE-1531834. The authors also thank Professor Thomas Staley for heat treatment of the door handle and railing and Matthew Ducker for help with the statistical analysis. The authors thank Mr. Majid Hosseini for the design and preparation of the cover art. This work was supported by the National Science Foundation under grant no. CBET-1902364, the Health and Medical Research Fund (COVID190116), and the National Institute of Allergy and Infectious Diseases (contract HHSN272201400006C).

REFERENCES

(1) COVID-19 Dashboard by the Center for Systems Science and Engineering (CSSE) at Johns Hopkins University (JHU). https://coronavirus.jhu.edu/map.html (accessed Oct 30, 2020).

(2) CDC Cleaning and Disinfection for Households. https://www.cdc.gov/coronavirus/2019-ncov/prevent-getting-sick/cleaning-disinfection.html (accessed Aug 30, 2020).

(3) Wilson, N. M.; Norton, A.; Young, F. P.; Collins, D. W. Airborne transmission of severe acute respiratory syndrome coronavirus-2 to healthcare workers: a narrative review. *Anaesthesia* 2020, *75*, 1086−1095.

(4) Otter, J. A.; Donskey, C.; Yezli, S.; Douthwaite, S.; Goldenberg, S. D.; Weber, D. J. Transmission of SARS and MERS coronaviruses and influenza virus in healthcare settings: the possible role of dry surface contamination. *J. Hosp. Infect.* 2016, *92*, 235−250.

(5) Sia, S. F.; Yan, L.-M.; Chin, A. W. H.; Fung, K.; Choy, K.-T.; Wong, A. Y. L.; Kaewpreedee, P.; Perera, R. A. P. M.; Poon, L. L. M.; Nicholls, J. M.; Peiris, M.; Yen, H.-L. Pathogenesis and transmission of SARS-CoV-2 in golden hamsters. *Nature* 2020, *583*, 834−838.

(6) Chin, A. W. H.; Poon, L. L. M.; Perera, M.; Hui, K.; Yen, H.-L.; Chan, M.; Peiris, M.; Poon, L. Stability of SARS-CoV-2 in different environmental conditions Authors' reply. *Lancet Microbe* 2020, *1*, No. e146.

(7) Van Doremalen, N.; Bushmaker, T.; Morris, D. H.; Holbrook, M. G.; Gamble, A.; Williamson, B. N.; Tamin, A.; Harcourt, J. L.; Thornburg, N. J.; Gerber, S. I.; Lloyd-Smith, J. O.; de Wit, E.; Munster, V. J. Aerosol and surface stability of SARS-CoV-2 as compared with SARS-CoV-1. *N. Engl. J. Med.* 2020, *382*, 1564−1567.
(8) Fathizadeh, H.; Maroufi, P.; Momen-Heravi, M.; Dao, S.; Köse, Ş.; Ganbarov, K.; Pagliano, P.; Esposito, S.; Kafil, H. S. Protection and disinfection policies against SARS-CoV-2 (COVID-19). *Infez. Med.* 2020, *28*, 185−191.
(9) Derraik, J. G. B.; Anderson, W. A.; Connelly, E. A.; Anderson, Y. C. Rapid Review of SARS-CoV-1 and SARS-CoV-2 Viability, Susceptibility to Treatment, and the Disinfection and Reuse of PPE, Particularly Filtering Facepiece Respirators. *Int. J. Environ. Res. Publ. Health* 2020, *17*, 6117.
(10) Behzadinasab, S.; Chin, A.; Hosseini, M.; Poon, L.; Ducker, W. A. A Surface Coating that Rapidly Inactivates SARS-CoV-2. *ACS Appl. Mater. Interfaces* 2020, *12*, 34723−34727.
(11) Ren, G.; Hu, D.; Cheng, E. W. C.; Vargas-Reus, M. A.; Reip, P.; Allaker, R. P. Characterisation of copper oxide nanoparticles for antimicrobial applications. *Int. J. Antimicrob. Agents* 2009, *33*, 587−590.
(12) Ahamed, M.; Alhadlaq, H. A.; Khan, M.; Karuppiah, P.; Al-Dhabi, N. A. Synthesis, characterization, and antimicrobial activity of copper oxide nanoparticles. *J. Nanomater.* 2014, *2014*, 637858.
(13) Chen, X.; Ku, S.; Weibel, J. A.; Ximenes, E.; Liu, X.; Ladisch, M.; Garimella, S. V. Enhanced antimicrobial efficacy of bimetallic porous CuO microspheres decorated with Ag nanoparticles. *ACS Appl. Mater. Interfaces* 2017, *9*, 39165−39173.
(14) Applerot, G.; Lellouche, J.; Lipovsky, A.; Nitzan, Y.; Lubart, R.; Gedanken, A.; Banin, E. Understanding the antibacterial mechanism of CuO nanoparticles: revealing the route of induced oxidative stress. *Small* 2012, *8*, 3326−3337.
(15) Azam, A.; Ahmed, A. S.; Oves, M.; Khan, M.; Memic, A. Size-dependent antimicrobial properties of CuO nanoparticles against Gram-positive and -negative bacterial strains. *Int. J. Nanomed.* 2012, *7*, 3527.
(16) Hans, M.; Mathews, S.; Mücklich, F.; Solioz, M. Physicochemical properties of copper important for its antibacterial activity and development of a unified model. *Biointerphases* 2015, *11*, 018902.
(17) Mittapally, S.; Taranum, R.; Parveen, S. Metal ions as antibacterial agents. *J. Drug Deliv. Therapeut.* 2018, *8*, 411−419.
(18) Semisch, A.; Ohle, J.; Witt, B.; Hartwig, A. Cytotoxicity and genotoxicity of nano-and microparticulate copper oxide: role of solubility and intracellular bioavailability. *Part. Fibre Toxicol.* 2014, *11*, 1−16.
(19) SMARTLAB. *Material Safety Data Sheet Copper(II) Oxide*, 2018.
(20) *ASTM, A. D3359-17 Standard Test Methods for Rating Adhesion by Tape Test*; ASTM International: West Conshohocken, PA, 2017.
(21) Malenovska, H. Virus quantitation by transmission electron microscopy, TCID50, and the role of timing virus harvesting: A case study of three animal viruses. *J. Virol. Methods* 2013, *191*, 136−140.
(22) Chan, K. H.; Lai, S. T.; Poon, L. L. M.; Guan, Y.; Yuen, K. Y.; Peiris, J. S. M. Analytical sensitivity of rapid influenza antigen detection tests for swine-origin influenza virus (H1N1). *J. Clin. Virol.* 2009, *45*, 205−207.
(23) Reed, L. J.; Muench, H. A Simple Method of Estimating Fifty per Cent Endpoints12. *Am. J. Epidemiol.* 1938, *27*, 493−497.
(24) Zhang, Q.; Zhang, K.; Xu, D.; Yang, G.; Huang, H.; Nie, F.; Liu, C.; Yang, S. CuO nanostructures: synthesis, characterization, growth mechanisms, fundamental properties, and applications. *Prog. Mater. Sci.* 2014, *60*, 208−337.
(25) Zhou, K.; Wang, R.; Xu, B.; Li, Y. Synthesis, characterization and catalytic properties of CuO nanocrystals with various shapes. *Nanotechnology* 2006, *17*, 3939.
(26) Ethiraj, A. S.; Kang, D. J. Synthesis and characterization of CuO nanowires by a simple wet chemical method. *Nanoscale Res. Lett.* 2012, *7*, 70.
(27) Wang, W. Z.; Wang, G. H.; Wang, X. S.; Zhan, Y. J.; Liu, Y. K.; Zheng, C. L. Synthesis and characterization of Cu2O nanowires by a novel reduction route. *Adv. Mater.* 2002, *14*, 67−69.
(28) Biesinger, M. C. Advanced analysis of copper X-ray photoelectron spectra. *Surf. Interface Anal.* 2017, *49*, 1325−1334.
(29) Hari Prasad Reddy, M.; Pierson, J. F.; Uthanna, S. Structural, surface morphological, and optical properties of nanocrystalline Cu2 O and CuO films formed by RF magnetron sputtering: Oxygen partial pressure effect. *Phys. Status Solidi A* 2012, *209*, 1279−1286.
(30) Janas, J.; Gurgul, J.; Socha, R. P.; Dzwigaj, S. Effect of Cu content on the catalytic activity of CuSiBEA zeolite in the SCR of NO by ethanol: Nature of the copper species. *Appl. Catal., B* 2009, *91*, 217−224.
(31) Polak, M.; Ohl, A.; Quaas, M.; Lukowski, G.; Lüthen, F.; Weltmann, K.-D.; Schröder, K. Oxygen and Water Plasma-Immersion Ion Implantation of Copper into Titanium for Antibacterial Surfaces of Medical Implants. *Adv. Eng. Mater.* 2010, *12*, B511−B518.
(32) Iijima, Y.; Niimura, N.; Hiraoka, K. Prevention of the Reduction of CuO during X-ray Photoelectron Spectroscopy Analysis. *Surf. Interface Anal.* 1996, *24*, 193−197.
(33) Parmigiani, F.; Pacchioni, G.; Illas, F.; Bagus, P. S. Studies of the Cu O bond in cupric oxide by X-ray photoelectron spectroscopy and ab initio electronic structure models. *J. Electron Spectrosc. Relat. Phenom.* 1992, *59*, 255−269.
(34) Baillot, R.; Deshayes, Y. *Reliability Investigation of LED Devices for Public Light Applications*; Elsevier, 2017.
(35) Zhang, J.; Liu, J.; Peng, Q.; Wang, X.; Li, Y. Nearly monodisperse Cu2O and CuO nanospheres: preparation and applications for sensitive gas sensors. *Chem. Mater.* 2006, *18*, 867−871.
(36) Borkow, G.; Gabbay, J. Copper, an ancient remedy returning to fight microbial, fungal and viral infections. *Curr. Chem. Biol.* 2009, *3*, 272−278.
(37) Luo, J.; Hein, C.; Mücklich, F.; Solioz, M. Killing of bacteria by copper, cadmium, and silver surfaces reveals relevant physicochemical parameters. *Biointerphases* 2017, *12*, 020301.
(38) Dasari, T. P.; Pathakoti, K.; Hwang, H.-M. Determination of the mechanism of photoinduced toxicity of selected metal oxide nanoparticles (ZnO, CuO, Co3O4 and TiO2) to E. coli bacteria. *J. Environ. Sci.* 2013, *25*, 882−888.
(39) Sunada, K.; Minoshima, M.; Hashimoto, K. Highly efficient antiviral and antibacterial activities of solid-state cuprous compounds. *J. Hazard. Mater.* 2012, *235*−*236*, 265−270.
(40) Meghana, S.; Kabra, P.; Chakraborty, S.; Padmavathy, N. Understanding the pathway of antibacterial activity of copper oxide nanoparticles. *RSC Adv.* 2015, *5*, 12293−12299.
(41) Hans, M.; Erbe, A.; Mathews, S.; Chen, Y.; Solioz, M.; Mücklich, F. Role of copper oxides in contact killing of bacteria. *Langmuir* 2013, *29*, 16160−16166.
(42) Liu, Z.; Xiao, X.; Wei, X.; Li, J.; Yang, J.; Tan, H.; Zhu, J.; Zhang, Q.; Wu, J.; Liu, L. Composition and divergence of coronavirus spike proteins and host ACE2 receptors predict potential intermediate hosts of SARS-CoV-2. *J. Med. Virol.* 2020, *92*, 595−601.
(43) Bianchi, M.; Benvenuto, D.; Giovanetti, M.; Angeletti, S.; Ciccozzi, M.; Pascarella, S. SARS-CoV-2 Envelope and Membrane Proteins: Structural Differences Linked to Virus Characteristics? *BioMed Res. Int.* 2020, *2020*, No. 4389089.
(44) Song, G.; Hou, W.; Gao, Y.; Wang, Y.; Lin, L.; Zhang, Z.;Niu, Q.; Ma, R.; Mu, L.; Wang, H. Effects of CuO nanoparticles on Lemna minor. *Bot. Stud.* 2015, *57*, 1−8.
(45) Prasad, S.; Potdar, V.; Cherian, S.; Abraham, P.; Basu, A.; Team, I.-N. N. Transmission electron microscopy imaging of SARS-CoV-2. *Indian J. Med. Res.* 2020, *151*, 241.
(46) Goldsmith, C. S.; Tatti, K. M.; Ksiazek, T. G.; Rollin, P. E.; Comer, J. A.; Lee, W. W.; Rota, P. A.; Bankamp, B.; Bellini, W. J.; Zaki, S. R. Ultrastructural characterization of SARS coronavirus. *Emerg. Infect. Dis.* 2004, *10*, 320.
(47) Xie, X.; Li, Y.; Sun, H.; Liu, L. Exhaled droplets due to talking and coughing. *J. R. Soc. Interface* 2009, *6*, S703−S714.

https://dx.doi.org/10.1021/acsami.0c19465
ACS Appl. Mater. Interfaces 2021, 13, 5919−5928

(48) Johnson, G. R.; Morawska, L.; Ristovski, Z. D.; Hargreaves, M.; Mengersen, K.; Chao, C. Y. H.; Wan, M. P.; Li, Y.; Xie, X.; Katoshevski, D.; Corbett, S. Modality of human expired aerosol size distributions. *J. Aerosol Sci.* 2011, *42*, 839−851.
(49) Yang, S.; Lee, G. W. M.; Chen, C.-M.; Wu, C.-C.; Yu, K.-P. The size and concentration of droplets generated by coughing in human subjects. *J. Aerosol Med.* 2007, *20*, 484−494.
(50) Morawska, L.; Johnson, G. R.; Ristovski, Z. D.; Hargreaves, M.; Mengersen, K.; Corbett, S.; Chao, C. Y. H.; Li, Y.; Katoshevski, D. Size distribution and sites of origin of droplets expelled from the human respiratory tract during expiratory activities. *J. Aerosol Sci.* 2009, *40*, 256−269.
(51) Papineni, R. S.; Rosenthal, F. S. The size distribution of droplets in the exhaled breath of healthy human subjects. *J. Aerosol Med.* 1997, *10*, 105−116.
(52) Han, Z. Y.; Weng, W. G.; Huang, Q. Y. Characterizations of particle size distribution of the droplets exhaled by sneeze. *J. R. Soc. Interface* 2013, *10*, 20130560.
(53) Scharfman, B.; Techet, A.; Bush, J.; Bourouiba, L. Visualization of sneeze ejecta: steps of fluid fragmentation leading to respiratory droplets. *Exp. Fluid* 2016, *57*, 24.
(54) Rantonen, P. J. F.; Meurman, J. H. Viscosity of whole saliva. *Acta Odontol. Scand.* 1998, *56*, 210−214.
(55) Gittings, S.; Turnbull, N.; Henry, B.; Roberts, C. J.; Gershkovich, P. Characterization of human saliva as a platform for oral dissolution medium development. *Eur. J. Pharm. Biopharm.* 2015, *91*, 16−24.
(56) Deegan, R. D.; Bakajin, O.; Dupont, T. F.; Huber, G.; Nagel, S. R.; Witten, T. A. Capillary flow as the cause of ring stains from dried liquid drops. *Nature* 1997, *389*, 827−829.
(57) Deegan, R. D.; Bakajin, O.; Dupont, T. F.; Huber, G.; Nagel, S. R.; Witten, T. A. Contact line deposits in an evaporating drop. *Phys. Rev. E: Stat., Nonlinear, Soft Matter Phys.* 2000, *62*, 756.
(58) Weon, B. M.; Je, J. H. Capillary force repels coffee-ring effect. *Phys. Rev. E: Stat., Nonlinear, Soft Matter Phys.* 2010, *82*, 015305.
(59) Cui, L.; Zhang, J.; Zhang, X.; Huang, L.; Wang, Z.; Li, Y.; Gao, H.; Zhu, S.; Wang, T.; Yang, B. Suppression of the coffee ring effect by hydrosoluble polymer additives. *ACS Appl. Mater. Interfaces* 2012, *4*, 2775−2780.
(60) Benavente, D.; Lock, P.; Angeles García Del Cura, M.; Ordoñez, S. Predicting the capillary imbibition of porous rocks from microstructure. *Transp. Porous Media* 2002, *49*, 59−76.
(61) Huber, P.; Grüner, S.; Schäfer, C.; Knorr, K.; Kityk, A. V. Rheology of liquids in nanopores: A study on the capillary rise of water, n-Hexadecane and n-Tetracosane in mesoporous silica. *Eur. Phys. J.: Spec. Top.* 2007, *141*, 101−105.
(62) Li, K.; Horne, R. N. An analytical scaling method for spontaneous imbibition in gas/water/rock systems. *SPE J.* 2004, *9*, 322−329.
(63) Cai, J.; Yu, B. A discussion of the effect of tortuosity on the capillary imbibition in porous media. *Transp. Porous Media* 2011, *89*, 251−263.
(64) Prat, M. On the influence of pore shape, contact angle and film flows on drying of capillary porous media. *Int. J. Heat Mass Transfer* 2007, *50*, 1455−1468.
(65) Ratanadecho, P.; Aoki, K.; Akahori, M. Influence of irradiation time, particle sizes, and initial moisture content during microwave drying of multi-layered capillary porous materials. *J. Heat Transfer* 2002, *124*, 151−161.

https://dx.doi.org/10.1021/acsami.0c19465
ACS Appl. Mater. Interfaces 2021, 13, 5919−5928